

Article

Green Synthesis of Flowerball-like MoS₂/VC Nanocomposite and Its Efficient Catalytic Performance for Oxygen Reduction Either in Alkaline or Acid Media

Xiaofeng Zhang ¹, Yayun Ke ¹, Ting Wang ¹, Jiannan Cai ¹, Qiufeng Huang ¹  and Shen Lin ^{2,3,*}

¹ College of Chemistry and Materials Science, Fujian Normal University, Fuzhou 350007, China; xfz_fz@163.com (X.Z.); keyy1058@163.com (Y.K.); wt071421@163.com (T.W.); asw19931126@163.com (J.C.); qiufenghuang@fjnu.edu.cn (Q.H.)

² Fujian Provincial Key Laboratory of Polymer Materials, Fujian Normal University, Fuzhou 350007, China

³ Fujian Provincial Key of Advanced Materials Oriented Chemical Engineering, Fujian Normal University, Fuzhou 350007, China

* Correspondence: shenlin@fjnu.edu.cn

Abstract: Opening up electrocatalysts for oxygen reduction reaction (ORR) is essential for practical application in fuel cells and metal-air batteries; however, how to make the catalysts with both good performance and low cost is difficult. Recently, research on the ORR of molybdenum disulfide-based catalysts in alkaline electrolytes has been on the rise. However, the development of MoS₂ catalyst for acidic ORR is still in its infancy. Herein, without using reductant and morphology control reagent, we firstly obtained flowerball-like MoS₂/Vulcan XC-72R (VC) nanocomposites via hydrothermal method. The designed composite exhibits a nearly 4e⁻ ORR process with 0.78 and 0.92 V onset potentials in 0.1 M KOH and HClO₄, respectively. Furthermore, the flowerball-like composite shows utmost electrochemical stability judging by 87 and 80% current retention for about 5.5 h either in alkaline or acid media, long term durability for continuous 10,000 cycles, and stronger resistance to methanol than the commercial Pt/C catalyst. The abundant Mo edges as catalytic active centers of flowerball-like structure, high electron conductivity, and enhanced mass transport in either alkaline or acidic electrolyte are favorable for catalytic performance. The prepared catalyst provides great potential for the substitution of noble metal based catalysts in fuel cells and metal-air batteries.

Keywords: flowerball-like; molybdenum disulfide; electrocatalysis; oxygen reduction reaction; alkaline; acid



Citation: Zhang, X.; Ke, Y.; Wang, T.; Cai, J.; Huang, Q.; Lin, S. Green Synthesis of Flowerball-like MoS₂/VC Nanocomposite and Its Efficient Catalytic Performance for Oxygen Reduction Either in Alkaline or Acid Media. *Catalysts* **2022**, *12*, 259. <https://doi.org/10.3390/catal12030259>

Academic Editors: Vincenzo Vaiano and Olga Sacco

Received: 27 January 2022

Accepted: 21 February 2022

Published: 25 February 2022

Publisher's Note: MDPI stays neutral with regard to jurisdictional claims in published maps and institutional affiliations.



Copyright: © 2022 by the authors. Licensee MDPI, Basel, Switzerland. This article is an open access article distributed under the terms and conditions of the Creative Commons Attribution (CC BY) license (<https://creativecommons.org/licenses/by/4.0/>).

1. Introduction

Fuel cells and metal-air batteries have attracted much attention owing to the demand for an environment-friendly conversion system and energy storage [1]. The reaction mechanism of a fuel cell and metal-air battery is oxidation-reduction reaction, and both of the cathode reaction are oxygen reduction reaction (ORR). However, fuel cells and metal-air batteries are inseparable from the use of catalysts, and the current lack of high-performance and low-cost ORR catalysts make them unable to achieve large-scale practical applications [2,3]. At present, the electrocatalysts for ORR mainly fall into four categories: platinum group metal (PGM or noble) catalysts, non-PGM catalysts, carbon-based catalysts, and single-atom-based catalysts [4,5]. Although PGM or noble catalysts have great advantages in ORR activity among alkaline and acid electrolytes, it is not the best choice in terms of price or durability. These serious problems hinder their further development. In order to realize the large-scale application of fuel cells and metal-air batteries, there is an urgent need to develop excellent performance for non-noble metal replacement catalysts. In other words, non-PGM catalysts need to have high electrocatalytic activity and long-term stability [6,7].

In recent years, the graphene-like transition metal dichalcogenides (TMDCs) have been widely acclaimed for their layered structure and low cost. Additionally, they are an environment-friendly material [8,9]. In particular, MoS₂ has a unique two-dimensional layered structure and exhibits outstanding thermal, electrical, and catalytic properties, therefore, it has been proposed to be a very promising electrocatalyst for ORR among TMDCs' family [10,11]. However, the catalytic activity of pristine MoS₂ in acidic media is still far from what is expected, as a result of the low density of active sites [12]. It is firstly reported that ultrathin MoS₂ layers were prepared by ultrasonically exfoliated method and used as ORR electrocatalyst. It is also found that their catalytic activity is size-dependent [13]. There are a large number of Mo atoms at the edge of MoS₂ with layered structure, which can be served as the active site for the adsorption of molecular oxygen. Water and hydroxyl ions may easily be reduced respectively under acidic or alkaline condition [14]. Meanwhile, porous structure and the specific surface area of carbon-based TMDCs have a large correlation to the reachability of the active sites and ORR activity [15–18]. Accordingly, it is highly desired to develop porous carbon structures rich in MoS₂ active sites.

In addition, studies have shown that a suitable support can effectively improve the activity of TMDCs catalysts. So far, Vulcan XC-72R (VC) is still the most common, simple, and stable catalyst support in PEMFCs on account of its wide commercial practicability, excellent chemical stability, and relatively large specific surface area. Moreover, the high conductivity of VC could further promote the electron transfer in the ORR process [19]. VC can not only be a commonly used support to load catalytic materials for ORR [20,21], but also shows certain activity for ORR by itself [22].

Herein, we report a flowerball-like MoS₂ without using reductant and morphology control reagent. This synthesis strategy could prevent the agglomeration of MoS₂ layers simply and effectively. Consequently, the as-prepared MoS₂/VC nanocomposite exhibits excellent performance against ORR in alkaline or acidic solution, whether in terms of activity, stability, or resistance to methanol. The specially improved ORR activity is beneficial from the uniform flowerball-like MoS₂ distributing onto porous carbon, which is capable of providing abundant Mo edges as catalytic active center for ORR.

2. Results and Discussion

XRD patterns (Figure 1) displays as-synthesized MoS₂ and MoS₂/C. Diffraction peaks centered at 14.38°, 32.68°, 33.51°, 39.54°, and 58.33° can be indexed to (002), (100), (101), (103), and (110) planes of hexagonal MoS₂ (2H-MoS₂, JCPDS 01-1201) [23,24], respectively. According to the Bragg equation ($2d\sin\theta = n\lambda$, $\lambda = 0.15418$ nm for Cu K α), the interplanar distance of MoS₂ (002) in the composite material is calculated to be mainly 0.62 nm, which further confirms that the synthesized sample is ordinary hexagonal MoS₂.

As shown in Figure 2, SEM images of different magnification exhibits flowerball-like shape of MoS₂. TEM image (Figure 3A) further illustrates that the MoS₂ dispersed with a size distribution of 200 ± 20 nm in diameter, and the MoS₂ reveals flowerball-like shape composed of nanoflakes (Figure 3B). The HR-TEM picture (Figure 3C) displays the clear crystal fringes of MoS₂ with a lattice spacing of 0.62 nm on the MoS₂ (002) plane, which is consistent with the result of XRD.

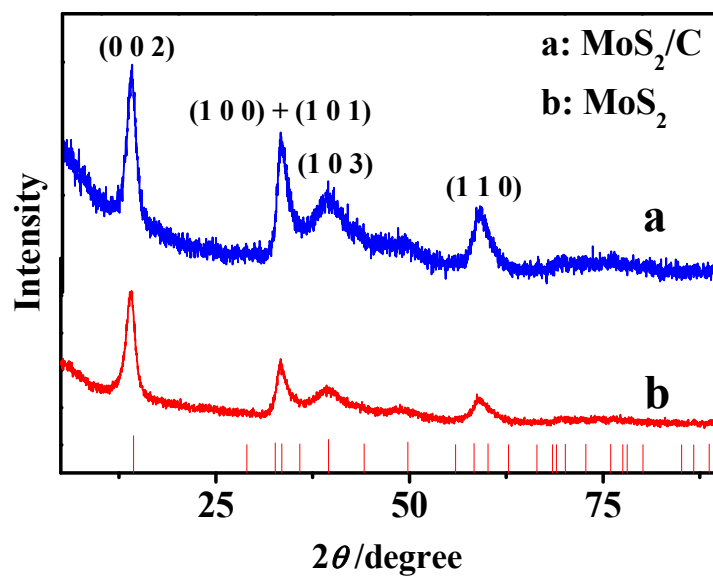


Figure 1. XRD patterns of the MoS₂/C, MoS₂, and the standard spectrum of MoS₂ (JCPDS No. 01-1201).

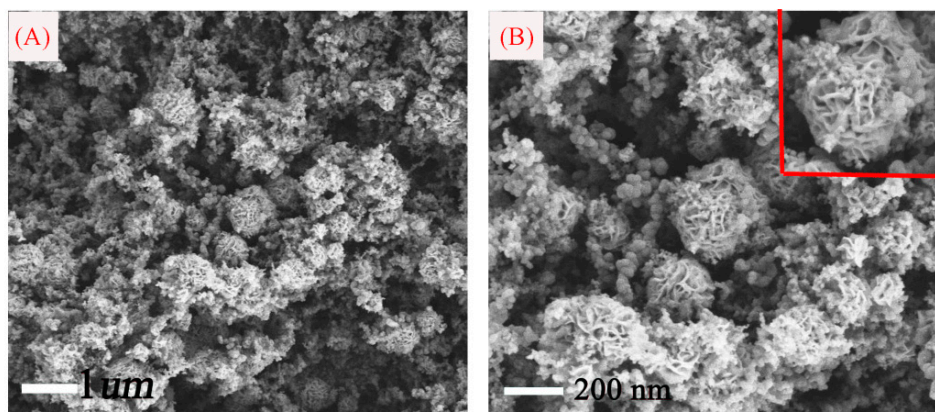


Figure 2. SEM images of MoS₂/C nanocomposites at different magnification: 1000 magnification (A) and 20,000 magnification (B).

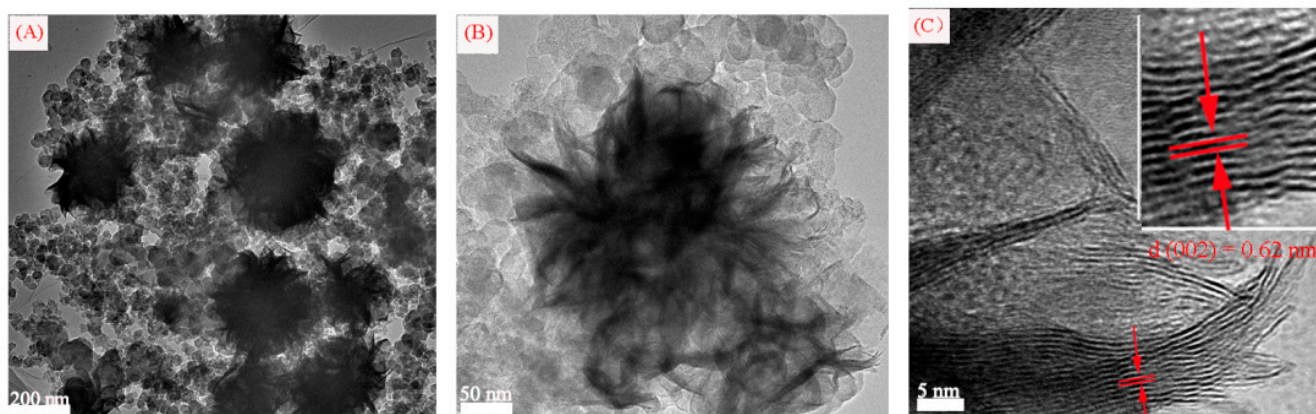


Figure 3. TEM images of MoS₂/C nanocomposites at different magnification (A–C). The inset is the HRTEM image.

XPS and EDS spectra of MoS₂/C nanocomposites are shown in Figure 4. The survey scan (Figure 4a) reveals the signal peaks of Mo3d, Mo3p, S2p, C1s, and O1s, manifesting the existence of Mo, S, and C elements. The existence of O may come from the raw material sodium molybdate dihydrate (Na₂MoO₄·2H₂O). The high-resolution Mo3d spectrum chart (Figure 4b) can appear as several peaks. Two strong characteristic peaks at 228.8 and 232.0 eV are assigned to Mo3d_{3/2} and Mo3d_{5/2} [24], respectively. A relative weak peak appearing at the binding energy of 232.5 eV is also identified to Mo3d_{5/2}. All these peaks show +4 oxidation state of Mo. Moreover, a weak broad peak at the binding energy of 235.8 eV belongs to +6 oxidation state of Mo [25], which may come from residual Na₂MoO₄·2H₂O. The results above suggest that Mo in the composite is mainly in the form of +4. In addition, the weak signal peak at the binding energy of 226.0 eV is the characteristic signal peak of S2s [23]. The S2p spectrum of MoS₂/C can be showed two peaks at 162.6 eV, 163.9 eV (Figure 4c), which is assigned to S2p_{1/2} and S2p_{3/2}, respectively. There is also a weak signal peak at the binding energy of 163.6 eV, which also belongs to S2p_{1/2}. All these data reveal that S exists in -2 oxidation state [26]. The presence of Mo and S peaks can be clearly observed from the EDS spectrum (Figure 4d), which indicates that the composite material contains Mo and S elements. It can be seen from EDS that the atomic ratio of Mo/S is almost 1:2, which confirms that the atomic ratio of MoS₂ is 1:2.

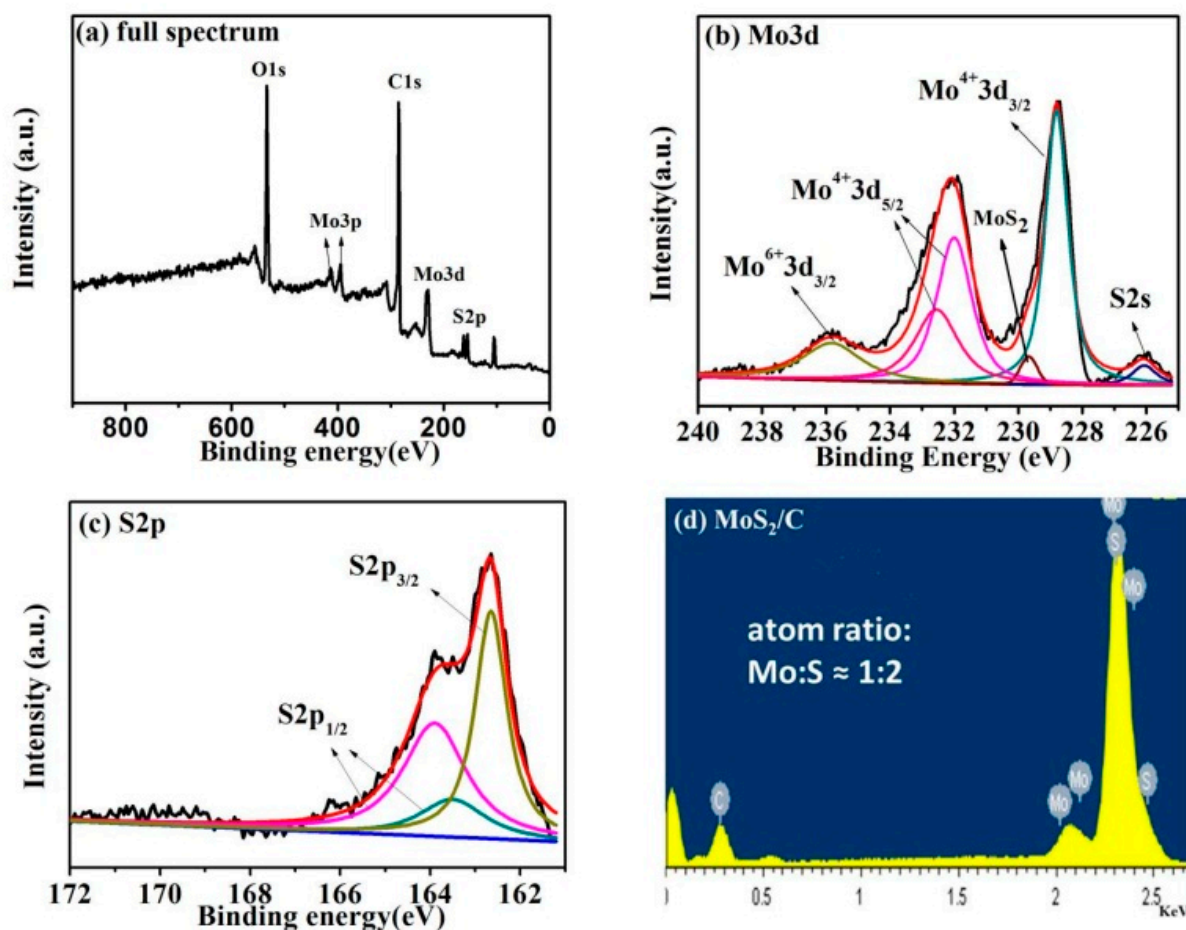


Figure 4. XPS and EDS spectra of the MoS₂/C composite: (a) full spectrum; (b) Mo3d spectrum; (c) S2p spectrum; (d) EDS spectrum.

It can be found from N₂-adsorption/desorption isotherms results (Figure 5) that the synthesized MoS₂/C composite possess higher adsorption capacity than pristine MoS₂. The surface areas of Vulcan C, pure MoS₂ sheets, and MoS₂/C composite measured by Brunauer-Emmett-Teller (BET) are 302.4 m² g⁻¹, 50.8 m² g⁻¹, and 184.5 m² g⁻¹, respectively,

indicating that MoS₂ nanosheets are dispersed in Vulcan C, which leads to an increase in the surface area of MoS₂.

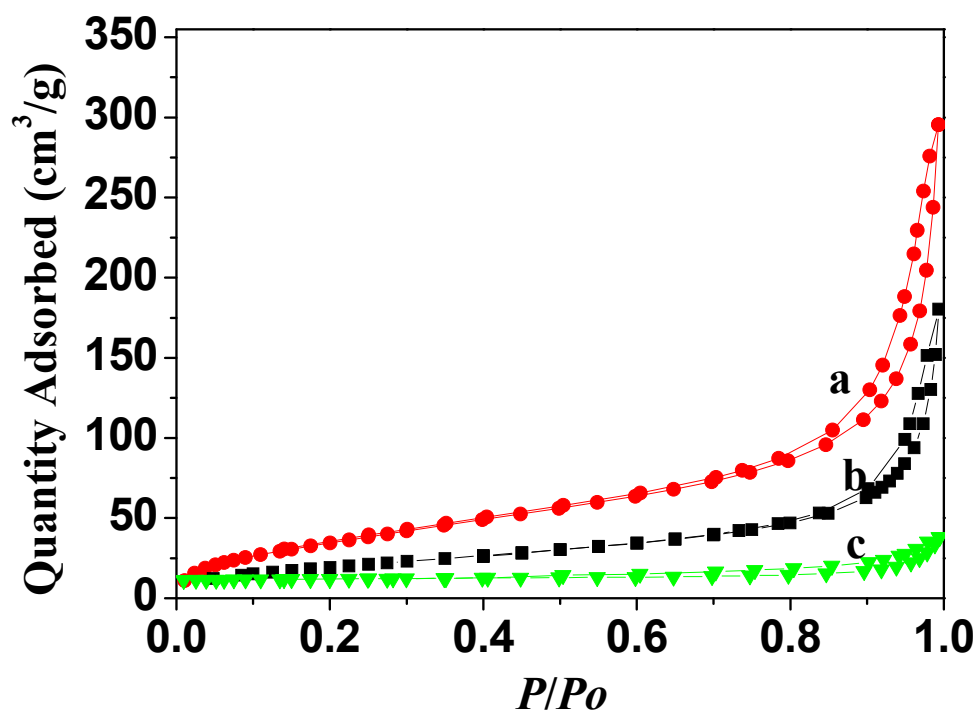


Figure 5. BET spectrum of the (a) VulcanXC-72R, (b) MoS₂/C composite, and (c) MoS₂.

The amount of C may have effects on the ORR catalytic performance of the composite. In this experiment, by adjusting the amount of C, the catalytic performances of MoS₂/C composites with different proportion are investigated through CV and LSV techniques in O₂ saturated 0.1 M KOH solution with the above operations to explore the optimal composition of the catalyst. Figure S1 displays CVs of MoS₂/C-15, MoS₂/C-20, MoS₂/C-25, and MoS₂/C-30. There are strong redox peaks at the potential of 0.77, 0.76, 0.82, and 0.78 V (vs. RHE), respectively. In contrast, there is no information about typical oxidation peaks in CVs recorded in N₂ saturated electrolyte. It should be noted that the oxygen reduction peak current density and onset potential of MoS₂/C-25 composite is the highest. It is necessary to further study the electrochemical kinetic properties of MoS₂/C composites on ORR, LSVs are recorded in O₂ saturated 0.1 M aqueous KOH electrolyte at a scan rate of 10 mV s⁻¹ with a rotational rate of 1600 rpm. Figure S2 shows comparative LSVs of MoS₂/C-15, MoS₂/C-20, MoS₂/C-25, and MoS₂/C-30 composites. The onset potential is one of the vital arguments to assess electrocatalytic activity for ORR. The starting potentials of MoS₂/C-15, MoS₂/C-20, MoS₂/C-25, and MoS₂/C-30 are found to be 0.74, 0.78, 0.82, and 0.75 V, respectively. Obviously, the MoS₂/C-25 composite displays the highest onset potential (0.82 V) and half-wave potential (0.71 V) with the increase of limiting current density (5.34 mA cm⁻²), suggesting the highest electrocatalytic activity for ORR compared to other MoS₂/C composites.

According to linear-sweep voltammetry (LSV), results at different rotational speeds, the Koutecky-Levich diagrams (K-L, j^{-1} vs. $\omega^{-1/2}$) were used to calculate the corresponding number of transferred electrons in ORR (Equations (3) and (4)). The LSV curves of the MoS₂/C-15, MoS₂/C-20, MoS₂/C-25, and MoS₂/C-30 composites at different rotation speeds are shown in Figure S3, which displays the calculated K-L plots for the four composites at a potential range of 0.4 to 0.2 V (vs. RHE, Figure 6). By calculating the slope of the K-L curve, the electron transfer number n of MoS₂/C-25 is 3.90 (vs. RHE), indicating that it is higher than MoS₂/C-15 (3.67), MoS₂/C-20 (3.69), and MoS₂/C-30 (3.84). The nearby

four electrons transferred per O₂ molecule (n) further supports the excellent performance of flowerball-like MoS₂/C-25.

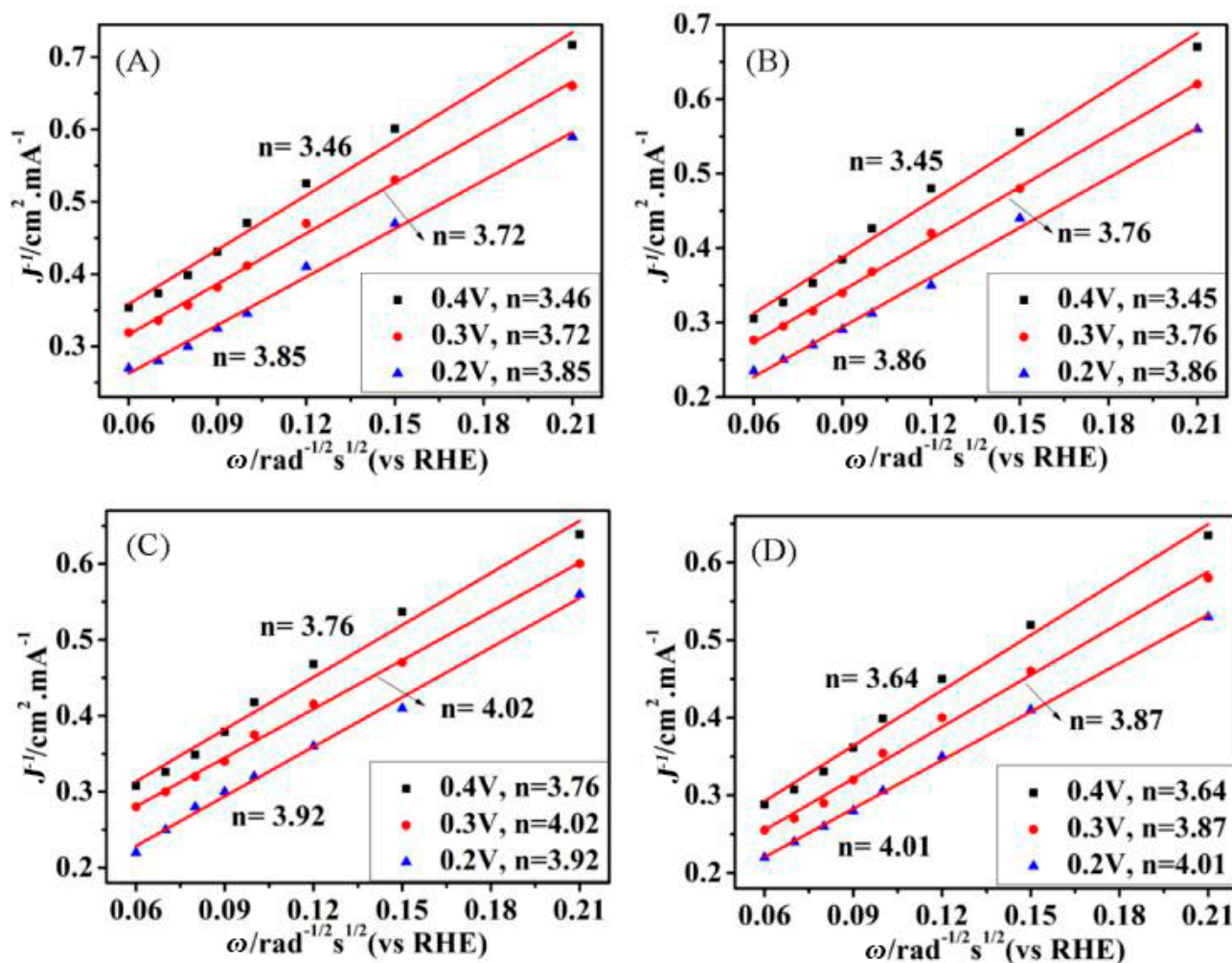


Figure 6. Koutecky-Levich plots for the MoS₂/C-15 (A), MoS₂/C-20 (B), MoS₂/C-25 (C), and MoS₂/C-30 (D) at different electrode potentials.

Figure 7 presents RRDE plots of MoS₂/C-25 and commercial Pt/C in 0.1 M KOH solution. Figure 7A,B are the ring currents (above) and disk current (below) currents of MoS₂/C-25 and commercial Pt/C at different rotating speeds, respectively. Therefore, it can be known that the ring current and disk current of MoS₂/C-25 and commercial Pt/C increase with the increase of speed. Figure 7C is the polarization curves of MoS₂/C-25 (a) and commercial Pt/C (b) at 1600 rpm. Although MoS₂/C-25 is not as good as commercial Pt/C in terms of initial potential and limiting current density value, the MoS₂/C-25 composite has made great progress in these two aspects compared to other reference data [23,24]. Figure 7D reveals the electron transfer number “n” and “HO₂[−] yield” calculated by the Formulas (3) and (4) curves by the RRDE curves at 1600 rpm. As observed, the HO₂[−] yield on the MoS₂/C-25 composite is below 20%. Moreover, the number of ascertained electron transfer during ORR process of the MoS₂/C-25 composite is 3.75, which further confirms that the ORR procedure experiences nearly four electron pathways over the composite. For non-noble metal based catalysts, a lower HO₂[−] yield is advisable because it not only improves ORR efficiency, but also prevents corrosive hydrogen peroxide damaging the catalysts.

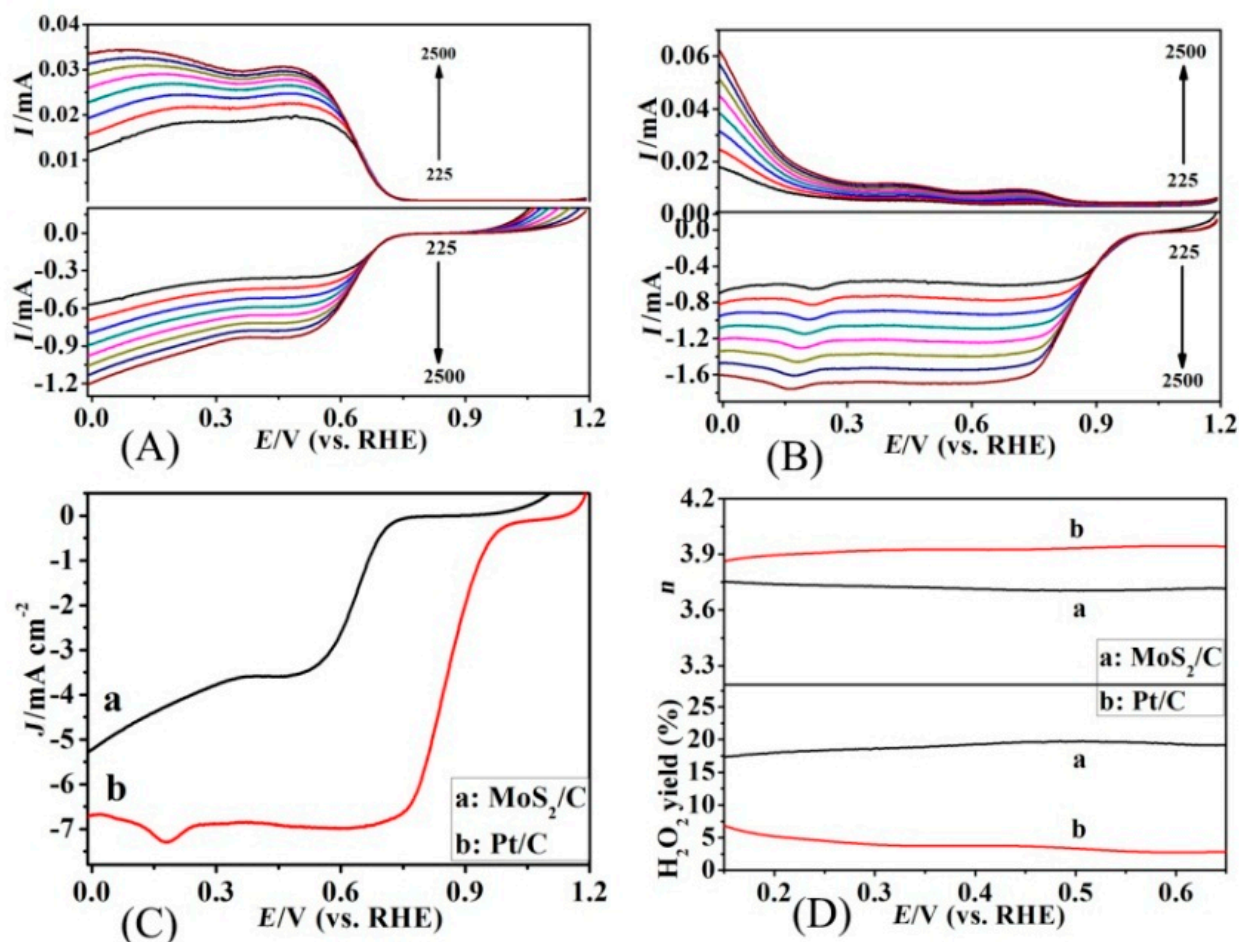


Figure 7. RRDE plots of different modified electrode: (A) MoS₂/C-25, (B) Pt/C; RRDE plots of different modified electrode: (C) RDE plots of (a) MoS₂/C-25 and (b) Pt/C in O₂-saturated 0.1 M KOH solution at rotation rate of 1600 rpm; (D) H₂O₂ yield measured and electron transfer number (n) of (a) MoS₂/C-25 and (b) Pt/C in O₂-saturated 0.1 M KOH at room temperature with rotation rate of 1600 rpm. Scan rate: 10 mVs⁻¹.

To further investigate the potential application of MoS₂/C-25 composite in acidic PEMFCs, the electrocatalytic activity of MoS₂/C-25 for ORR is also judged in 0.1 M HClO₄. According to Figure S4, in the alkaline solutions, the peak potential of oxygen reduction of MoS₂/C-25 is 0.82 V and the corresponding current density is 0.67 mA cm⁻². It can be seen from Figure S4B in 0.1M HClO₄ electrolyte solution saturated with oxygen, the peak potential of oxygen reduction of MoS₂/C-25 is 0.81 V, and the corresponding current density is 0.75 mA cm⁻². The CV results show that the MoS₂/C-25 composite also possesses ORR activity in acidic solutions.

Figure 8 shows the RRDE plots of MoS₂/C-25 and existing Pt/C in 0.1 M HClO₄ solution. From Figure 8A,B, we can find that the ring currents and disk currents of MoS₂/C-25 and commercial Pt/C both increase with the increase of rotating speed. Accordingly, the polarization curve of MoS₂/C-25 (a) at 1600 rpm in Figure 8C reveals that the MoS₂/C-25 has an onset potential of 0.90 V (vs. RHE), which is comparable with that of Pt/C (0.93 V vs. RHE) and exhibits a diffusion-limited current (j_L) of 7.39 mA cm⁻², indicating that MoS₂/C-25 obtains more current, compared to the current obtained by commercial Pt/C (5.84 mA cm⁻²). Importantly, the electron transfer number “n” on the MoS₂/C-25 composite is 3.98, which is higher than that of Pt/C (3.76). The “H₂O₂ yield” on the MoS₂/C-25 composite is close to zero, which indicates that the reduction of O₂ to H₂O in acid medium is via four-electrons pathway over this composite. The above results further indicate that

the MoS₂/C-25 composite material performs better than commercial Pt/C catalysts in terms of catalytic activity, selectivity, and stability for ORR in acidic medium.

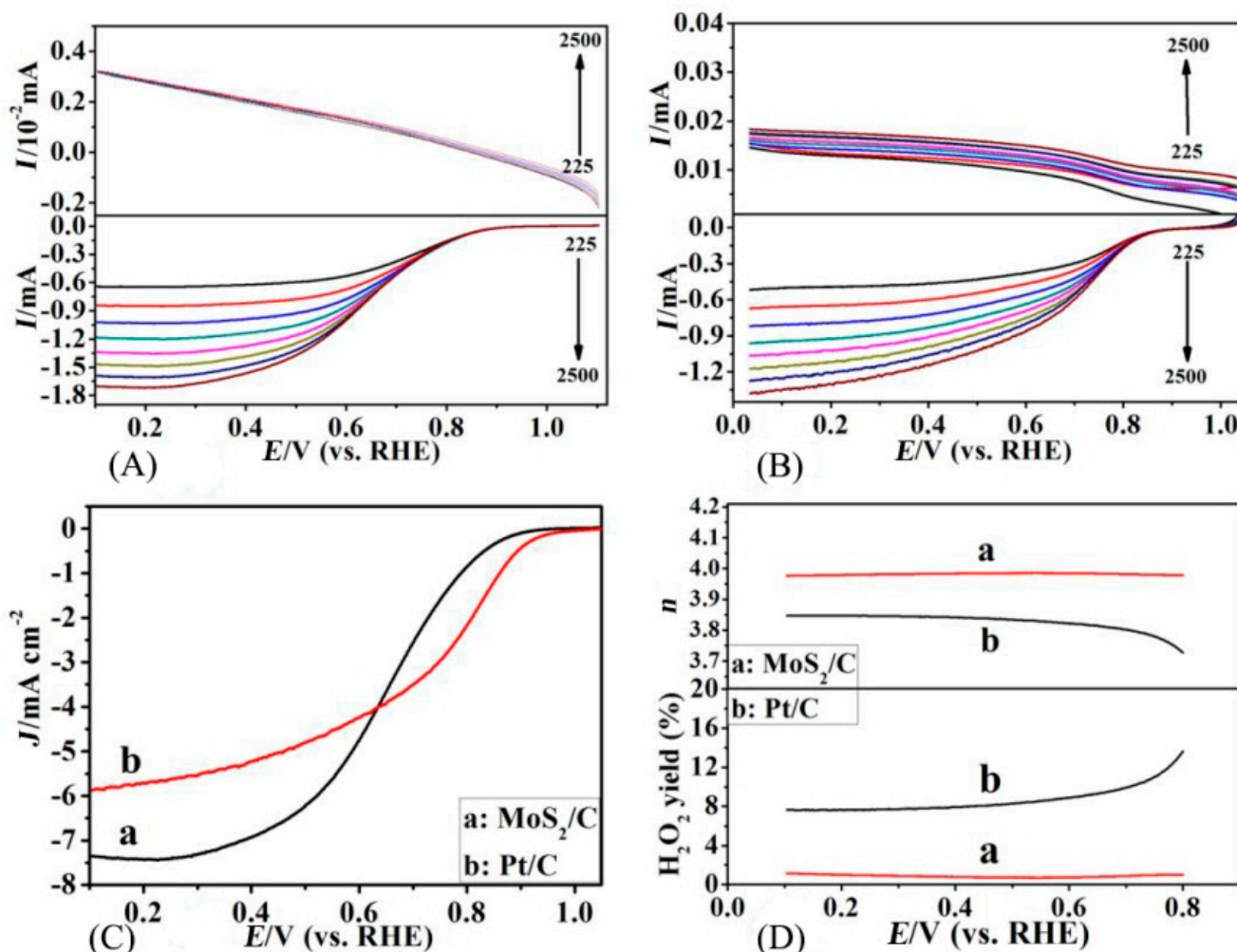


Figure 8. RRDE plots of different modified electrode: (A) MoS₂/C-25, (B) Pt/C at different rotation rate; (C) LSV curves of the MoS₂/C -25 (a) and Pt/C (b) in O₂-saturated 0.1 M HClO₄ solution at rotation rate of 1600 rpm; (D) H₂O₂ yield measured and electron transfer number (n) using (a) MoS₂/C-25 and (b) Pt/C as a catalyst, respectively, in O₂-saturated 0.1 M HClO₄ with rotation rate of 1600 rpm. Scan rate: 10 mVs⁻¹.

Furthermore, the as-prepared flowerball-like MoS₂/VC here are also compared with recently reported MoS₂-based graphene [11,15], N,S co-doped carbon composites [27], or carbon nanotubes hybrid materials [28]: MoS₂/NG, MoS₂/graphene, MoS₂@NSC, and MoS₂-CNT (Table S1, ESI†). Although the onset potential of the MoS₂/VC (0.82 V vs. RHE) in 0.1 M KOH is lower than that of MoS₂/graphene (0.91 V vs. RHE) and MoS₂@NSC (0.93 V vs. RHE), the limiting current density is higher than that of MoS₂/graphene and MoS₂@NSC, and close to that of MoS₂-CNT, suggesting the enhancement of electrochemical activity of flowerball-like MoS₂/VC in alkaline medium. Moreover, it can be seen from Table S1 that the synthesized MoS₂/VC exhibits better oxygen reduction catalytic activity in acidic medium than that under alkaline condition. The comparison further proves that flowerball-like MoS₂/VC can be used as an excellent catalyst for ORR under both alkaline and acidic condition. The reason maybe as follows: The flower structure effectively inhibited the stacking of MoS₂ layers. Electrocatalytic ORR active sites of MoS₂ is realized by the presence of abundant Mo edges in the layered structures, which serve as preferred active sites for the adsorption of molecular oxygen and its subsequent reduction to the

desired by-products such as water and hydroxyl ions in acid and in alkaline conditions, respectively [29].

One important factor to enhance electrocatalytic performance is the superior electric conductivity of the composite, which can be proven by Nyquist plots of the electrochemical impedance spectrum (EIS). The EIS curves of MoS₂/C, MoS₂, and VulcanXC-72R in 0.1 M KOH/0.1 M HClO₄ electrolyte are revealed in Figure S5. In Figure S5, MoS₂/C, MoS₂, and VulcanXC-72R all exhibit obvious semicircles in the high-frequency region. It is generally believed that the result of the high frequency semicircle diameter is equal to the charge transfer resistance (Rct) [30]. In the base or acid media, the Rct of MoS₂/C composite is both obviously smaller than that of MoS₂ or VulcanXC-72R. In addition, the Rct of MoS₂/C composite in acid medium is even smaller than that in alkaline medium. The result indicates that electrons transfer easier in acid medium, which is also reflected in the experimental results of CV and RRDE.

Besides, the ability of tolerance to methanol is also a significant criterion of a superior electrocatalyst for fuel cell. The as-prepared MoS₂/C composite was tested by CV scans in O₂-saturated 0.1 M KOH with 10 vol% methanol (Figure 9). The value of the oxygen reduction current hardly changes in 0.1 M KOH or 0.1 M HClO₄ solution. This indicates that the MoS₂/C composite exhibits high selectivity for ORR to avoid crossover effect both in base and acid media. By comparison, Pt/C changes significantly after the addition of methanol, which is manifested as a methanol oxidation reaction, indicating that Pt/C is highly sensitive to methanol infiltrated from anode in fuel cells.

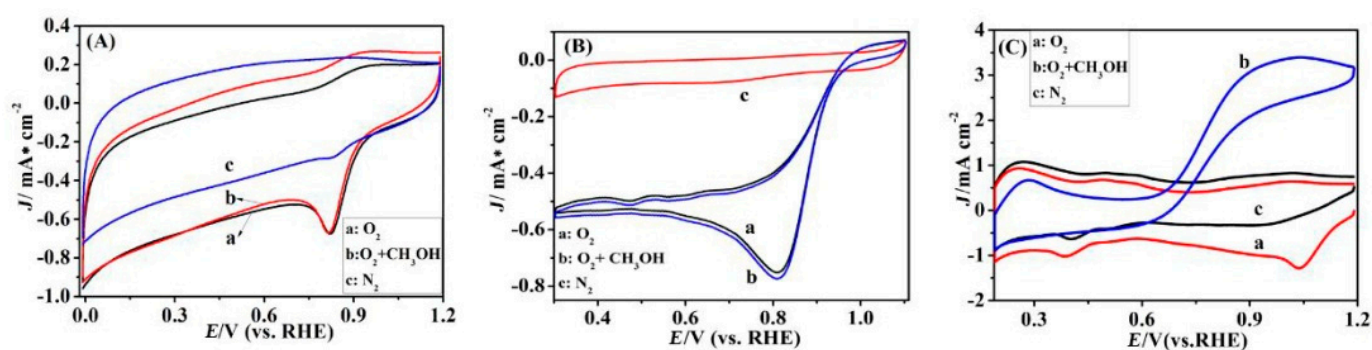


Figure 9. CVs in N₂/O₂-saturated and O₂-saturated 0.1 M KOH/0.1 M HClO₄ upon the addition of CH₃OH (10 vol%) for (A) MoS₂/C in 0.1 M KOH and (B) MoS₂/C in 0.1 M HClO₄ and (C) Pt/C in 0.1 M KOH. Scan rate: 30 mV s⁻¹.

The chronoamperometric curves (i-t, Figure S6a,b) of as-prepared MoS₂/C display a slow attenuation and retain 87 and 80% of original current in 0.1 M KOH or 0.1 M HClO₄ solution after 20,000 s. In contrast, after the experiment was carried out for 20,000 s, the current loss of MoS₂ was 32%, and Pt/C also gradually decreased, and the current loss was about 47%. The result distinctly indicates that the prepared MoS₂/C has high durability, which is better than Pt/C catalyst. In addition, after 10,000 cycles from 0.4 to 1.2 V, it can be observed that the ORR peak potential and current density of MoS₂/C in 0.1 M KOH (Figure 10A) hardly change. The same is true in 0.1 M HClO₄ solution (Figure 10B). The ORR peak potential of Pt/C (Figure 10C) has shifted by nearly 50 mV and the current density has been reduced by nearly two times, which further reveal that the MoS₂/C composite possesses higher stability and is better than Pt/C catalyst.

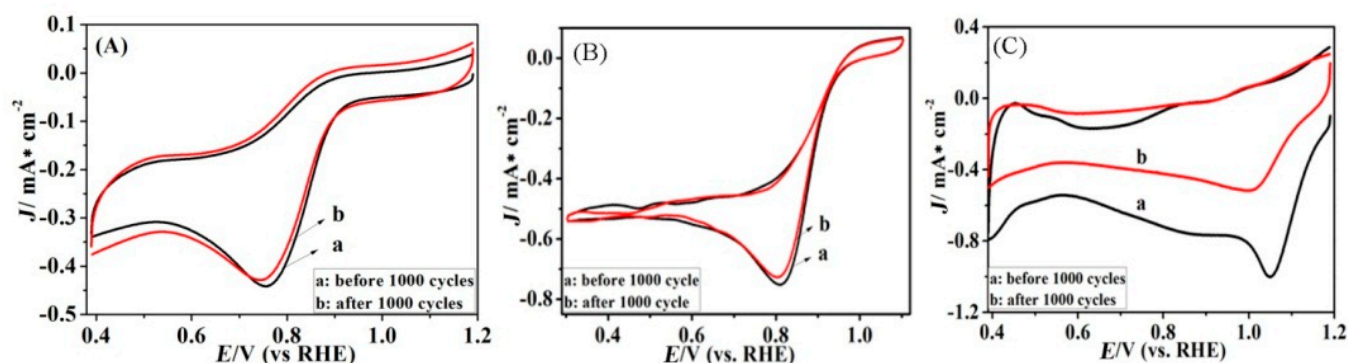


Figure 10. Continuous cyclic voltammograms of different modified electrodes: (A) MoS₂/C composite, (B) in O₂-saturated 0.1 HClO₄ solution, and (C) Pt/C in O₂-saturated 0.1 M KOH solution. Scan rate: 20 mV s⁻¹.

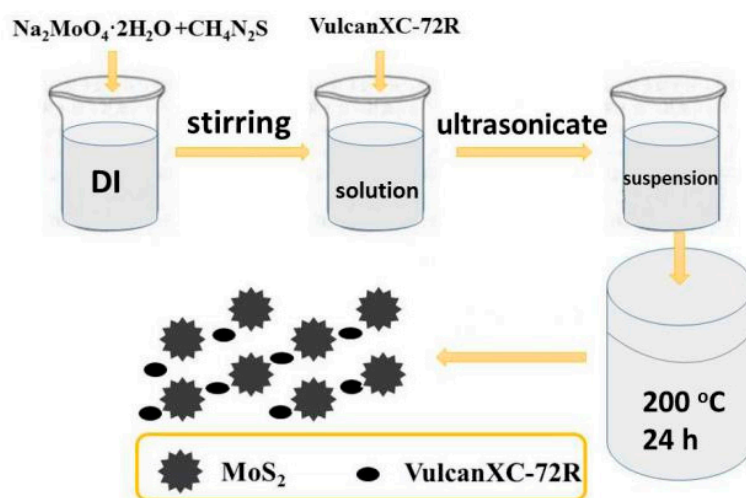
3. Experimental

3.1. Reagents and Chemicals

Sodium molybdate dihydrate (Na₂MoO₄·2H₂O), thiourea (CH₄N₂S), potassium hydroxide (KOH), perchloric acid (HClO₄), methanol, ethanol, and isopropanol were obtained from Sinopharm Chemical Reagent Co., Ltd. Vulcan XC-72R was obtained from Cabot (Boston, MA, USA). Commercial 20% Pt/C catalyst was acquired from Alfa Aesar. Nafion[®] 117 solution was purchased from Aldrich. All reagents were used as received without further purification.

3.2. Synthesis of MoS₂/VC Composite

Typical one-plot synthesis of MoS₂/Vulcan XC-72R composite (MoS₂/C) was described in Scheme 1 (all reagents used in the preparation are of analytical pure grade). As illustrated in Scheme 1, 1 mmol Na₂MoO₄·2H₂O and 2 mmol CH₄N₂S were added in 35 mL of deionized (DI) water with stirring. Then, 25 mg VC was added into the above solution. The resulted mixture was ultrasonicated for 1 h. Then, it was added into 100 mL Teflon-lined stainless steel autoclave in 200 °C for 24 h. The as-prepared black powder was centrifugal washed with DI water and ethanol. Finally, it dried at 60 °C under vacuum. For comparison, 15, 20, and 30 mg of VC were also considered for synthesis and the obtained samples were denoted as MoS₂/C-15, MoS₂/C-20, and MoS₂/C-30, respectively.



Scheme 1. Schematic preparation of MoS₂/C composites.

3.3. Physicochemical Characterization

Phase analysis of materials was observed by XRD (X-ray diffractometer, Siemens D5005, Berlin, Germany) in Cu K α radiation. XPS (X-ray photoelectron spectroscopy, Quantum-2000 Scanning ESCA Microprobe system, Chanhassen, MN, USA) were carried out to analyze the valence state of element, which is tested in the excitation source of Al mono K radiation at the pass energy of 46.95 eV. The scanning electron microscopy (SEM, JEOL 7500F, Hitachi, Tokyo, Japan) and transmission electron microscopy (TEM, Philips TECNAI G2, 200 KV, FEI, Hillsboro, OR, USA) were tested to observe the size and morphology of materials. The Brunner-Emmet-Teller (BET, Coulter Omnisorp 100cx analyzer, Brea, CA, USA) was used to obtain the specific surface area.

3.4. Electrochemical Measurements

In ORR test, the relevant electrochemical characterization was performed on an electrochemical workstation (CHI 660E). Electrode material preparation: The glassy carbon electrode (GCE, 5 mm in diameter, Pine Research Instruments) was served as working electrode; counter electrode is a graphite rods, and reference electrode uses saturated Ag/AgCl (3 M KNO₃) with double junction.

All potentials would be referred to RHE. As follows:

$$E_{\text{RHE}} = E_{\text{Ag/AgCl}} + 0.962 \text{ V (0.1 M KOH)} \quad (1)$$

$$E_{\text{RHE}} = E_{\text{Ag/AgCl}} + 0.303 \text{ V (0.1 M HClO}_4) \quad (2)$$

Pre-treatment of GCE: The GCE was firstly polished by α -Al₂O₃ with particle size of 1.0, 0.3, and 0.05 μm , respectively, and then washed with distilled water. Afterwards, it was ultrasonicated with anhydrous ethanol and DI for about 1–2 min, respectively. Cyclic voltammetry was used to scan repeatedly in 0.5 M H₂SO₄ solution (−0.25 V~1.0 V (vs. Ag/AgCl)) until it reached a stable state. After that, it was washed with DI, and dried slowly with N₂.

Pre-treatment of catalyst: 5 mg catalyst was dispersed in a mixed solution (0.3 mL isopropanol (IPA), 0.6 mL DI, 0.1 mL 5% Nafion[®] 117 solution (Alfa Aesar)). Next, 3.6 μL dispersion solution were coated on the treated GCE, and dried naturally.

Electrochemical test: (1) Cyclic voltammetry (CV) curve: 0.1 M HClO₄ (acidic medium) or 0.1 M KOH (alkaline medium) was used as an electrolyte (passing through O₂/N₂ to saturation (about 45 min)). The treated electrodes were penetrated into the solution, and the scanning range was −1.0~0.2 V (vs. Ag/AgCl) (acidic medium: −0.4~0.8 V (vs. Ag/AgCl)). The scanning rate was 100, 80, 50, 30, 20, 10 mV s^{−1} to obtain CV curves, respectively. (2) Rotating ring disk (RRDE) curve: The rotational speeds were 225, 400, 625, 900, 1225, 1600, 2025, and 2500 rpm, respectively. (3) Continuous CV curves were tested in O₂ saturated 0.1 M KOH (or 0.1 M HClO₄) solution with scanning intervals ranging from −0.6 to 0.2 V (vs. Ag/AgCl) (acidic medium: 0 to 0.8 V (vs. Ag/AgCl)), scanning speed of 20 mV s^{−1}, and continuous scanning of 10000 cycles. (4) Methanol tolerance test was performed in a mixture solution of 0.1 M KOH (or 0.1 M HClO₄) and 10% methanol. The electrochemical impedance (EIS) was conducted in 0.1 M KOH (or 0.1 M HClO₄) solution at a fixing current density. The time-current (i–t) curve was performed in O₂ saturated 0.1 M KOH (or 0.1 M HClO₄) solution for 20,000 s.

The rotating ring-disk electrode technique (RRDE) could be also used to determine electron transfer number (n) and the production of H₂O₂ toward ORR. The correlation formulas is as follows:

$$n = 4I_{\text{D}} / (I_{\text{D}} + I_{\text{R}}/N) \quad (3)$$

$$\text{H}_2\text{O}_2\% = 200I_{\text{R}} / (NI_{\text{D}} + I_{\text{R}}) \quad (4)$$

In above formulas, I_D and I_R represent the ring current and the ring current. N represents collection efficiency (0.37).

4. Conclusions

In conclusion, the flowerball-like MoS₂/VC nanocomposites were successfully synthesized by hydrothermal method. The method is simple and does not need to use any reducing agent and morphology control agent. The addition of Vulcan XC-72 evidently enhances the electrical conductivity and specific surface area of MoS₂. The as-prepared MoS₂/VC nanocomposite with ball size of ca. 200 nm, and the catalyst can be uniformly dispersed on VC support. The uniform dispersion of flowerball-like MoS₂ onto porous carbon provides abundant Mo edges as catalytic active centers for ORR, resulting in superior electrocatalytic performance for ORR either in alkaline or acidic media. Moreover, MoS₂/VC also exhibits significant electrochemical durability to ORR in alkaline or acidic media, and its performance is better than pure molybdenum disulfide catalysts. The production of more effective catalysts in alkaline or acidic media is the significance and paving the way for the successful application of defect engineering to ORR catalysts. Significant improvement of electrocatalytic performance for other electrocatalysts, such as WSe₂ and MoSe₂, can also be expected by designing Mo or W edges-rich structures.

Supplementary Materials: The following supporting information can be downloaded at: <https://www.mdpi.com/article/10.3390/catal12030259/s1>, Figure S1: Cyclic voltammograms of (A) MoS₂/C-15, (B) MoS₂/C-20, (C) MoS₂/C-25 and (D) MoS₂/C-30 in N₂ and O₂-saturated 0.1 M KOH solution. Scan rate: 30 mV s⁻¹; Figure S2: ORR polarization curves of different modified electrode: (a) MoS₂/C-15, (b) MoS₂/C-20, (c) MoS₂/C-25 and (d) MoS₂/C-30 in O₂-saturated 0.1 M KOH solution at 1600 rpm rotation rate; scan rate: 10 mV s⁻¹; Figure S3: LSV curves of the MoS₂/C-15 (A), MoS₂/C-20 (B), MoS₂/C-25 (C) and MoS₂/C-30 (D) in O₂-saturated 0.1 M KOH solution at different rotation rates; scan rate: 10 mV s⁻¹; Figure S4: CVs of MoS₂/C-25 in different solution: (A) O₂-saturated 0.1 M KOH solution; (B) O₂-saturated 0.1 M HClO₄ solution. Scan rate: 30 mV s⁻¹; Table S1: Comparison of the performance of MoS₂-based electrocatalysts for ORR; Figure S5: Nyquist plots of the different modified electrodes: (a) MoS₂/C in 0.1 M HClO₄ solution, (b) MoS₂/C, (c) VulcanXC-72R and (d) MoS₂ in 0.1 M KOH solution; Figure S6: Chronoamperometric curves of different modified electrodes: (a) MoS₂/C-base, (b) MoS₂/C-acid, (c) MoS₂ and (d) Pt/C in O₂-saturated 0.1 M KOH/0.1 M HClO₄ solution for 20,000 s.

Author Contributions: X.Z., Y.K. and T.W. did the experiments; X.Z. wrote the first draft; J.C. and Q.H. took part in the discussion of experiments results and revision of paper; S.L. was responsible for the research work and paper revision. All authors have read and agreed to the published version of the manuscript.

Funding: Authors gratefully acknowledge the funding of the National Natural Science Foundation of China (No. 21571034&22102028).

Conflicts of Interest: The authors declare no conflict of interest.

References

1. Ji, Y.; Dong, H.; Liu, C.; Li, Y. The progress of metal-free catalysts for the oxygen reduction reaction based on theoretical simulations. *J. Mater. Chem. A* **2018**, *6*, 13489–13508. [[CrossRef](#)]
2. Shao, M.; Chang, Q.; Dodelet, J.-P.; Chenitz, R. Recent advances in electrocatalysts for oxygen reduction reaction. *Chem. Rev.* **2016**, *116*, 3594–3657. [[CrossRef](#)] [[PubMed](#)]
3. Wang, W.; Jia, Q.; Mukerjee, S.; Chen, S. Recent insights into the oxygen-reduction electrocatalysis of Fe/N/C materials. *ACS Catal.* **2019**, *9*, 10126–10141. [[CrossRef](#)]
4. Tian, X.; Lu, X.F.; Xia, B.Y.; Lou, X.W. Advanced electrocatalysts for the oxygen reduction reaction in energy conversion technologies. *Joule* **2020**, *4*, 45–68. [[CrossRef](#)]
5. Chen, L.; Xu, X.; Yang, W.; Jia, J. Recent advances in carbon-based electrocatalysts for oxygen reduction reaction. *Chin. Chem. Lett.* **2020**, *31*, 626–634. [[CrossRef](#)]
6. Dai, L.; Xue, Y.; Qu, L.; Choi, H.-J.; Baek, J.-B. Metal-free catalysts for oxygen reduction reaction. *Chem. Rev.* **2015**, *115*, 4823–4892. [[CrossRef](#)]
7. Yi, J.-D.; Xu, R.; Wu, Q.; Zhang, T.; Zang, K.-T.; Luo, J.; Liang, Y.-L.; Huang, Y.-B.; Cao, R. Atomically dispersed iron-nitrogen active sites within porphyrinic triazine-based frameworks for oxygen reduction reaction in both alkaline and acidic media. *ACS Energy Lett.* **2018**, *3*, 883–889. [[CrossRef](#)]

8. Chia, X.; Lazar, P.; Sofer, Z.K.; Luxa, J.; Pumera, M. Layered SnS versus SnS₂: Valence and structural implications on electrochemistry and clean energy electrocatalysis. *J. Phys. Chem. C* **2016**, *120*, 24098–24111. [[CrossRef](#)]
9. Chua, X.J.; Luxa, J.; Eng, A.Y.S.; Tan, S.M.; Sofer, Z.K.; Pumera, M. Negative electrocatalytic effects of p-doping niobium and tantalum on MoS₂ and WS₂ for the hydrogen evolution reaction and oxygen reduction reaction. *ACS Catal.* **2016**, *6*, 5724–5734. [[CrossRef](#)]
10. Yang, X.; Jia, Q.; Duan, F.; Hu, B.; Wang, M.; He, L.; Song, Y.; Zhang, Z. Multiwall carbon nanotubes loaded with MoS₂ quantum dots and MXene quantum dots: Non-Pt bifunctional catalyst for the methanol oxidation and oxygen reduction reactions in alkaline solution. *Appl. Surf. Sci.* **2019**, *464*, 78–87. [[CrossRef](#)]
11. Arunchander, A.; Peera, S.G.; Sahu, A. Synthesis of flower-like molybdenum sulfide/graphene hybrid as an efficient oxygen reduction electrocatalyst for anion exchange membrane fuel cells. *J. Power Sources* **2017**, *353*, 104–114. [[CrossRef](#)]
12. Ramakrishnan, S.; Karuppanan, M.; Vinothkannan, M.; Ramachandran, K.; Kwon, O.J.; Yoo, D.J. Ultrafine Pt nanoparticles stabilized by MoS₂/N-doped reduced graphene oxide as a durable electrocatalyst for alcohol oxidation and oxygen reduction reactions. *ACS Appl. Mater. Interfaces* **2019**, *11*, 12504–12515. [[CrossRef](#)] [[PubMed](#)]
13. Wang, T.; Gao, D.; Zhuo, J.; Zhu, Z.; Papakonstantinou, P.; Li, Y.; Li, M. Size-dependent enhancement of electrocatalytic oxygen-reduction and hydrogen-evolution performance of MoS₂ particles. *Chem. A Eur. J.* **2013**, *19*, 11939–11948. [[CrossRef](#)] [[PubMed](#)]
14. Asadi, M.; Kumar, B.; Liu, C.; Phillips, P.; Yasaei, P.; Behranginia, A.; Zapol, P.; Klie, R.F.; Curtiss, L.A.; Salehi-Khojin, A. Cathode based on molybdenum disulfide nanoflakes for lithium-oxygen batteries. *ACS Nano* **2016**, *10*, 2167–2175. [[CrossRef](#)] [[PubMed](#)]
15. Zhao, K.; Gu, W.; Zhao, L.; Zhang, C.; Peng, W.; Xian, Y. MoS₂/Nitrogen-doped graphene as efficient electrocatalyst for oxygen reduction reaction. *Electrochim. Acta* **2015**, *169*, 142–149. [[CrossRef](#)]
16. Du, C.; Huang, H.; Feng, X.; Wu, S.; Song, W. Confining MoS₂ nanodots in 3D porous nitrogen-doped graphene with amendable ORR performance. *J. Mater. Chem. A* **2015**, *3*, 7616–7622. [[CrossRef](#)]
17. Zhou, J.; Xiao, H.; Zhou, B.; Huang, F.; Zhou, S.; Xiao, W.; Wang, D. Hierarchical MoS₂-rGO nanosheets with high MoS₂ loading with enhanced electro-catalytic performance. *Appl. Surf. Sci.* **2015**, *358*, 152–158. [[CrossRef](#)]
18. Huang, H.; Feng, X.; Du, C.; Wu, S.; Song, W. Incorporated oxygen in MoS₂ ultrathin nanosheets for efficient ORR catalysis. *J. Mater. Chem. A* **2015**, *3*, 16050–16056. [[CrossRef](#)]
19. Huang, H.; Zhang, X.; Zhang, Y.; Huang, B.; Cai, J.; Lin, S. Facile synthesis of laminated porous WS₂/C composite and its electrocatalysis for oxygen reduction reaction. *Int. J. Hydrog. Energy* **2018**, *43*, 8290–8297. [[CrossRef](#)]
20. Vega-Cartagena, M.; Rojas-Pérez, A.; Colón-Quintana, G.S.; Blasini Pérez, D.A.; Peña-Duarte, A.; Larios-Rodríguez, E.; De Jesús, M.A.; Cabrera, C.R. Potential dependent Ag nanoparticle electrodeposition on Vulcan XC-72R carbon support for alkaline oxygen reduction reaction. *J. Electroanal. Chem.* **2021**, *891*, 115242–115253. [[CrossRef](#)]
21. Lu, Y.; Zhao, S.; Yang, R.; Xu, D.; Yang, J.; Lin, Y.; Shi, N.-E.; Dai, Z.; Bao, J.; Han, M. Well-coupled nanohybrids obtained by component-controlled synthesis and in situ integration of Mn_xPd_y nanocrystals on Vulcan carbon for electrocatalytic oxygen reduction. *ACS Appl. Mater. Interfaces* **2018**, *10*, 8155–8164. [[CrossRef](#)] [[PubMed](#)]
22. Ma, Y.; Wang, H.; Ji, S.; Goh, J.; Feng, H.; Wang, R. Highly active Vulcan carbon composite for oxygen reduction reaction in alkaline medium. *Electrochim. Acta* **2014**, *133*, 391–398. [[CrossRef](#)]
23. Illathvalappil, R.; Unni, S.M.; Kurungot, S. Layer-separated MoS₂ bearing reduced graphene oxide formed by an in situ intercalation-cum-anchoring route mediated by Co(OH)₂ as a Pt-free electrocatalyst for oxygen reduction. *Nanoscale* **2015**, *7*, 16729–16736. [[CrossRef](#)] [[PubMed](#)]
24. Huang, H.; Feng, X.; Du, C.; Song, W. High-quality phosphorus-doped MoS₂ ultrathin nanosheets with amenable ORR catalytic activity. *Chem. Commun.* **2015**, *51*, 7903–7906. [[CrossRef](#)]
25. Ho, Y.T.; Ma, C.H.; Luong, T.T.; Wei, L.L.; Yen, T.C.; Hsu, W.T.; Chang, W.H.; Chu, Y.C.; Tu, Y.Y.; Pande, K.P. Layered MoS₂ grown on c-sapphire by pulsed laser deposition. *Phys. Status Solidi (RRL) Rapid Res. Lett.* **2015**, *9*, 187–191. [[CrossRef](#)]
26. Wei, L.; Chen, Y.; Lin, Y.; Wu, H.; Yuan, R.; Li, Z. MoS₂ as non-noble-metal co-catalyst for photocatalytic hydrogen evolution over hexagonal ZnIn₂S₄ under visible light irradiations. *Appl. Catal. B Environ.* **2014**, *144*, 521–527. [[CrossRef](#)]
27. Huang, M.; Chen, H.; He, J.; Chen, J.; Sun, L.; Li, Y.; Ren, X.; Deng, L. Synthesis of ultrathin MoS₂ nanosheets embedded in 3D hierarchically nitrogen-and-sulfur co-doped porous carbon composites as efficient oxygen reduction reaction catalyst. *ChemElectroChem* **2020**, *7*, 3260–3268. [[CrossRef](#)]
28. Lee, C.; Ozden, S.; Tewari, C.S.; Park, O.-K.; Vajtai, R.; Chatterjee, K.; Ajayan, P.M. MoS₂-carbon nanotube porous 3D network for enhanced oxygen reduction reaction. *ChemSusChem* **2018**, *11*, 2960–2966. [[CrossRef](#)]
29. Xu, H.; Zhu, J.; Ma, Q.; Ma, J.; Bai, H.; Chen, L.; Mu, S. Two-dimensional MoS₂: Structural properties, synthesis methods, and regulation strategies toward oxygen reduction. *Micromachines* **2021**, *12*, 240. [[CrossRef](#)]
30. Wang, W.; Kapitanova, O.O.; Ilanchezhian, P.; Xi, S.; Panin, G.N.; Fu, D.; Kang, T.W. Self-assembled MoS₂/rGO nanocomposites with tunable UV-IR absorption. *RSC Adv.* **2018**, *8*, 2410–2417. [[CrossRef](#)]